Journal of Applied Fluid Mechanics, Vol. 15, No. 2, pp. 579-589, 2022.
Available online at www.jafmonline.net, ISSN 1735-3572, EISSN 1735-3645.
https://doi.org/10.47176/jafm.15.02.33180

Comparative Numerical Study on Global Heat Transfer Process in Micro-Channel Gas Coolers with Different Structures

D. Yang, N. Wang, J. Xie† and J. Wang

College of Food Science and Technology, Shanghai Ocean University, China
Shanghai Professional Technology Service Platform on Cold Chain Equipment Performance and Energy Saving Testing Evaluation, China
Shanghai Engineering Research Center of Aquatic Product Processing & Preservation
National Experimental Teaching Demonstration Center for Food Science and Engineering (Shanghai Ocean University), China

†Corresponding Author Email: jxie@shou.edu.cn

(Received July 9, 2021; accepted October 15, 2021)

ABSTRACT

A numerical simulation of global heat transfer process in three types of micro-channel heat exchangers was investigated in this paper: spiral double-pipe micro-channel heat exchanger (DPHE), cross-plate micro-channel heat exchanger (CPHE), and shell and tube micro-channel heat exchanger (STHE). The inner tubes of all three heat exchangers have a diameter of 1 mm and are charged with CO_2 as refrigerant. A detailed analysis of the heat exchanger's global heat transfer process was carried out, which is entirely different for different structures. The heat transfer characteristics of supercritical CO_2 were analyzed by considering the operating pressure, the refrigerant mass flux, the cooling water mass flux, and the heat exchanger refrigerant inlet temperature. The relationship between the CO_2 heat transfer coefficient (h_{CO_2}) and CO_2 bulk temperature (T_{b,CO_2}) was analyzed in detail. The pseudo-critical temperature (T_{pc}) mainly determines where the peak CO_2 heat transfer coefficient occurs. When $T_{b,CO_2} < T_{pc}$, the rise in T_{b,CO_2} is accompanied by an increase in the heat transfer coefficient, which reaches a maximum when T_{b,CO_2} is a little bit higher than the pseudo-critical temperature, the heat transfer coefficient curve begins to decline as T_{b,CO_2} continues to rise. Higher peak heat transfer coefficients can be achieved at higher pressures. Increased refrigerant mass flux always results in larger heat transfer coefficients. The influence of the refrigerant inlet temperature of the heat exchanger in the $T_{b,CO_2} < T_{pc}$ region on the heat transfer coefficient is more significant than expected. In this study, different flow patterns on heat transfer due to different structures were compared. The best heat transfer was achieved using a spiral double-pipe micro-channel heat exchanger (DPHE). It consistently reaches the highest heat transfer and the lowest outlet temperature under the same operating conditions.

Keywords: Micro-channel heat exchanger; Supercritical CO_2; Heat transfer coefficient.

NOMENCLATURE

b	bulk	C_P	specific heat
G	mass flux	H	enthalpy
in	inner wall	h	heat transfer coefficient
k	conductivity	m	mass flow rate
o	outer wall	P	pressure
pc	preudo-critical	Q	heat exchange
q	heat flux	r	reference
T	temperature	u	velocity
w	wall	x	axial position
y	axial position	z	axial position
μ	viscosity		

1. INTRODUCTION

Trans-critical CO_2 (T-CO_2) refrigeration cycle is considered an efficient and environment-friendly system attributed to the complex properties of CO_2 near the critical point, widely used in automotive air conditioning, food refrigeration, and heat pumps (Eskandari and Cheraghi 2019). The gas cooler in T-CO_2) refrigeration cycle(Liang *et al.* 2020; Pan *et al.* 2020; Rigola *et al.* 2005; Wang *et al.* 2018) has to cool CO_2 from 373 K to 298 K at 8-10 MPa Nekså *et al*. (1998). The working condition is close to the critical point where the physical properties of CO_2 change drastically, which makes it challenging to design gas coolers. Therefore, the micro-channel heat exchanger is the most suitable gas cooler due to its pressure capacity (Kim and Bullard 2001).

Most of the research on heat exchangers has focused partly on automotive air conditioning (Li *et al.* 2017; Wang *et al.* 2018; Yang *et al.* 2019) limited by the higher air temperature of secondary flow and partly on printed circuit heat exchangers (Bennett *et al.* 2020; Katz *et al.* 2021; Kim *et al.* 2016; Saeed *et al.* 2020) limited by the high cost. Han *et al.* (2012) presented a review of the micro-channel heat exchanger development applied in an air-conditioning system. He pointed out the importance of accurately predicting pressure losses and heat transfer characteristics before designing micro-channel heat exchangers. The steep increase and decrease in specific heat and the sudden drop in density cause the heat transfer characteristic of CO_2 to be completely different from those substances with constant physical properties. Therefore, a large number of investigations have focused on the heat transfer characteristics of CO_2.

Jiang *et al.* (2008a,b,c) have done extensive research on the supercritical CO_2 heat transfer characteristics in vertical tubes. They noted that an increase in heat flux leads to a rise in heat transfer coefficient, but then the upward and downward flowing heat transfer coefficients move in the opposite direction when the heat flux continues to increase. Xu *et al.* (2015) experimentally compared the heat transfer in a small serpentine vertical tube and a straight tube. They concluded that the reason why the heat transfer performance of the serpentine tube is better than that of the straight tube is that the secondary flow due to the centrifugal force of the serpentine tube enhanced the heat transfer. Zhang *et al.* (2019b) conducted a numerical simulation study on the heat transfer characteristics of supercritical CO_2 in horizontal semicircular micro-tubes. It was found that specific heat would be in occupying more percentage in influencing the heat transfer process with an absence of buoyancy. Lei *et al.* (2019) did experiments in order to study the heat transfer characteristics of supercritical CO_2 in a small vertical circular tube, especially in the case of low mass flux and high heat flux. He found that the buoyancy force in the small channel plays a decisive role in heat transfer under such conditions.

As mentioned above, several heat transfer studies have been done in single tubes, where the boundary conditions are given a constant wall temperature and constant heat flux. Studies on supercritical CO_2 heat transfer mainly focus on the heat transfer characteristics of CO_2 in a tube. The boundary conditions are usually a given wall temperature and a constant heat flux. However, it is meaningful to look into water-cooled heat exchangers considering the applications in marine food transportation and heat pumps. The global and local heat transfer coefficients of two types of fluted tube heat exchangers and smooth tube heat exchangers were compared in an experiment by Zhu *et al.* (2019). The results showed that the global heat transfer coefficient of the smooth tube was only 1/3 of that of the fluted tube.

The most significant heat transfer coefficients were obtained for small hydraulic diameters regardless of the pressure. Wang *et al.* (2019) conducted experiments on the heat transfer characteristics of supercritical water in a tube-in-tube heat exchanger. The temperature corresponding to the peak heat transfer coefficient is not equal to the pseudo-critical temperature, and the higher the pressure, the more the temperature corresponding to the peak deviates from the pseudo-critical temperature. Cai *et al.* (2020a) and Ehsan *et al.* (2018) investigated experimentally and numerically the heat transfer of supercritical CO_2 in a micro-tube heat exchanger. He came to the same conclusion as Zhang *et al.* (2019a) and Wang *et al.* (2019) and Ma *et al.* (2016) that buoyancy has a significant effect on heat transfer at low Reynolds number. He also compared extra water flow of shell side process. The best heat transfer effect is achieved by counter-current flow. Most studies on microchannel gas coolers have focused on single-tube heat transfer, simulations of the overall global transfer process of microchannel heat exchangers has rarely been done, while simulation comparison of microchannel air coolers has not been done. For the reason the system we studied is a marine trans-critical CO_2 vapor compression cycle refrigeration system with ejectors, it is appropriate to use seawater as the cooling water in the gas cooler. Considering the corrosiveness of seawater and its susceptibility to scaling, shell and tube heat exchangers, double-pipe heat exchangers and cross-plate heat exchangers were preferred because they could be cleaned easily.

In this paper, three different structures of micro-channel gas coolers with an inner diameter of 1 mm to ensure the same heat transfer area on the CO_2 side have been selected according to the existing water-cooled heat exchanger structure on the market. (1) a spiral double-pipe heat exchanger (DPHE). (2) a cross-plate heat exchanger (CPHE). (3) a shell and tube heat exchanger (STHE). The heat transfer characteristics of supercritical CO_2 at different pressures, CO_2 mass flow rates, water mass flow rates, and CO_2 inlet temperatures were investigated numerically to find out the optimal structure of the water-cooled micro-channel heat exchanger.

2. NUMERICAL SIMULATION

2.1 Numerical Model

The structure and dimensions of the three types of micro-channel gas coolers were shown in Fig.1, the distribution of micro-channel in Fig.1a was referred to Guoqing (2015), and Fig.1b was referred to Fronk and Garimella (2011), Fig.1c considered available heat exchanger products on the market. x=0 mm and x=10 mm are the positions of CO_2 inlet and outlet in DPHE, respectively, the number of turns is 1, and the radius of rotation was 15 mm, as shown in Fig. 1. The flow of CO_2 and water was counter-current. The CPHE was designed as a seven-plate type with the CO_2 inlet at y=0 and the outlet at y=-8 mm. The flow of CO_2 and water was a cross-flow. z=0 mm and z=54 mm are the positions of CO_2 inlet and outlet in STHE respectively.

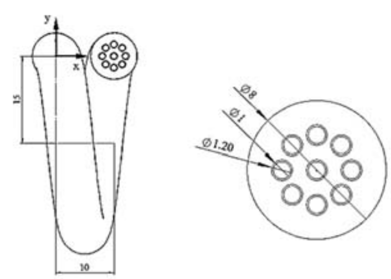

(a) DPHE

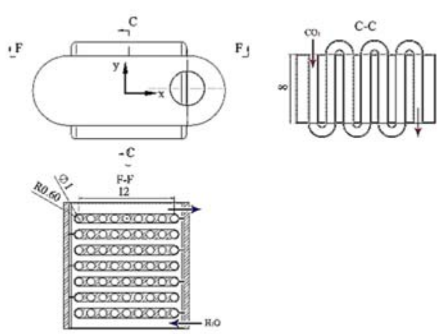

(b) CPHE

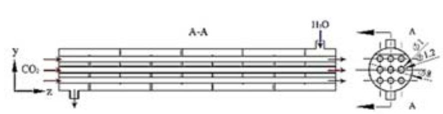

(c) STHE

Fig. 1. Numerical model.

The presence of the baffles ensured that the flow between CO_2 and water is counter-flow. The same tube diameter, number of tubes, and tube length are required for all three heat exchangers to ensure the same heat transfer area on the refrigerant side. Supercritical CO_2 flowed in 9 circular tubes with a diameter of 1 mm, while water flowed counter-current or cross-current on the shell side. There was a tube wall of 0.1 mm thickness between CO_2 and water. Following assumptions were required in the simulation:

1. uniform flow on the tube side.
2. uniform flow at the shell side inlet.
3. heat conduction exists only in the vertical direction of the tube wall.
4. ideal counter-flow or cross-flow between CO_2 and water.
5. the heat exchangers are placed horizontally.

The global heat transfer processes were simulated using ANSYS fluent 19.0 (Soloveva *et al.* 2021). SST k-ω turbulent model (Chen *et al.* 2018; Wang and Kissick 2020; Yang *et al.* 2018; Zhang *et al.* 2020) was selected in this paper. NIST refprop9.11 (Sanaye *et al.* 2020) was used to reference the properties. Mass-flow inlet and pressure-outlet were chosen as the boundary conditions. Table 1 shows the details of the simulated working conditions.

Table 1 The initial data for the simulations.

G_{co_2} $\left(\mathrm{kg/m^2s}\right)$	G_{water} $\left(\mathrm{kg/m^2s}\right)$	$T_{CO_2,in}$ (K)	P (MPa)	$T_{water,in}$ (K)
800	100	323.15	8	288.15
1000	159	343.15	9	
1200	238	373.15	10	

2.2 Governing Equations

A steady-state method was used in the simulation. The equation for conservation of mass, or continuity equation, can be written as Eq. 1.

$$\frac{\partial\left(\rho u_j\right)}{\partial x_j}=0 \tag{1}$$

Conservation of momentum is described by Eq. 2.

$$\frac{\partial}{\partial x_j}\left(\rho u_i u_j\right)=\frac{\partial}{\partial x_j}\left[\mu_{eff}\left(\frac{\partial u_i}{\partial x_j}+\frac{\partial u_j}{\partial x_i}\right)-\frac{2}{3}\mu_{eff}\frac{\partial u_k}{\partial x_k}\right]-\frac{\partial p}{\partial x_j}+\rho g_i \tag{2}$$

where μ_{eff} is the effective viscosity which is calculated as Eq. 3.

$$\mu_{eff}=\mu+\mu_t \tag{3}$$

where μ_t is the turbulent viscosity defined according to the turbulence model.

Conservation of energy is described by Eq. 4.

$$\frac{\partial\left(\rho u_i c_p T\right)}{\partial x_j} = \frac{\partial}{\partial x_j}\left[\begin{array}{l}\mu_{eff}\left(\frac{\partial u_i}{\partial x_j}+\frac{\partial u_j}{\partial x_i}\right) \\ -\frac{2}{3}\mu_{eff}\frac{\partial u_k}{\partial x_k}\end{array}\right] + \frac{\partial}{\partial x_i}\left(k_{eff}\frac{\partial T}{\partial x_i}\right) \quad (4)$$

where k_{eff} is the effective conductivity which is calculated as Eq. 5.

$$k_{eff} = k + k_t \quad (5)$$

where k_t is the turbulent thermal conductivity defined according to the turbulence model.

k - equation and ω- equation are described by Eq. 6 and Eq. 7.

$$\frac{\partial\left(\rho u_j k\right)}{\partial x_j} = \frac{\partial}{\partial x_j}\left(\mu+\frac{\mu_t}{\sigma_k}\right)\frac{\partial k}{\partial x_j} + P_k - D_k + S_k \quad (6)$$

$$\frac{\partial\left(\rho u_j \omega\right)}{\partial x_j} = \frac{\partial}{\partial x_j}\left(\mu+\frac{\mu_t}{\sigma_\omega}\right)\frac{\partial \omega}{\partial x_j} + C_\omega + P_\omega - D_\omega \quad (7)$$

2.3 Data Reduction

After the simulation is completed, the results of the inner and outer wall temperature and heat flux along the axial line can be output directly in STHE and CPHE. The bulk temperature of CO_2, the water temperature, and the heat transfer coefficient need to be calculated twice. All the above variables in DPHE are subject to a secondary calculation. The CO_2 heat transfer coefficient inside was calculated by

$$h_{CO_2} = \frac{q_{w,in}}{T_{b,CO_2} - T_{w,in}} \quad (8)$$

where $q_{w,in}$ and $T_{w,in}$ were the average wall heat flux and the internal wall temperature along the axial line, respectively, which were calculated by

$$q_{w,in} = \frac{\int qdL}{L} \quad (9)$$

$$T_{w,in} = \frac{\int TdL}{L} \quad (10)$$

L was the heat exchange pipe's length, the axial position in STHE is equal to z and y in CPHE. L in DPHE represents the direction along the helix. The CO_2 bulk temperature was calculated by

$$T_{b,CO_2} = \frac{\int \rho u c_p TdA}{\int \rho u c_p dA} \quad (11)$$

The water heat transfer coefficient was calculated by

$$h_{H_2O} = \frac{q_{w,out}}{T_{w,out} - T_{b,H_2O}} \quad (12)$$

where $q_{w,out}$ and $T_{w,out}$ were the average wall heat flux and the outer wall temperature along the axial line, respectively. The water temperature was calculated by

$$T_{b,H_2O} = \frac{\int \rho u c_p TdA}{\int \rho u c_p dA} \quad (13)$$

The total heat exchange was calculated as follows

$$Q_{exchange} = \dot{m}_{CO_2}\left(H_{CO_2,in} - H_{CO_2,out}\right) \quad (14)$$

2.4 Reliability Verification

2.4.1 Model Validation

Since experiments on supercritical CO_2 double-pipe heat exchangers have been done previously, this paper directly used the previously obtained experimental data to verify the validity of the simulation. The specific equipment of the experiments and the working conditions can be found in Ref. Yang *et al.* (2017). Figure 2 showed a comparison of the numerical and experimental results for different pressures. The SST k – ω turbulent model is proved to be accurate and reliable in the heat transfer prediction.

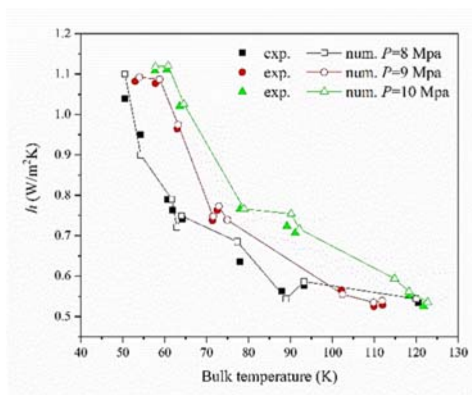

Fig. 2. Comparison of numerical calculation results with experimental results.

2.4.2 Grid Independence

Table 2. shows the pressure drop for different grid numbers. It can be seen that the pressure drop in the cross-plate heat exchanger is no longer significant for a grid partition of 2917110, and 3382495 for the shell and tube heat exchanger, 2245768 for the double-pipe heat exchanger. Therefore, grids with the numbers 2917110, 3382495, and 2245768 were selected to save computational time.

3. RESULTS AND DISCUSSIONS

3.1 Global Heat Transfer Processes

Figure 3ab shows the global heat transfer process in CPHE, including axial temperature, axial wall heat flux, and axial local CO_2 heat transfer coefficient. Only the first plate of the flow channel is intercepted for analysis because the global analysis of the cross-plate flow along the axial direction is complicated.

Table 2 Mesh independence verification.

cases	Number of meshes	Pressure drop	Error(%)
CPHE	1089997	1935.8	48.2
	1577912	1483	13.5
	2205040	1381	5.7
	2917110	1325.8	1.5
	3892329	1306.2	0
STHE	1032040	429.8	2.94
	1995913	426.2	2.09
	2579068	424.1	1.3
	3382495	433	0.49
	4213105	436.6	0
DPHE	839664	631.3	48.8
	1682660	466.6	10.0
	2245768	430.1	1.4
	3368652	424	0

The heat exchange process can be roughly divided into three parts in CPHE, based on the heat flux along the axial line in Fig. 3a: CO_2 inlet section, relatively stable section, and water inlet section. The high heat flux at the CO_2 inlet is attributed to the vast temperature difference between the refrigerant and cooling water and the higher CO_2 heat transfer coefficient caused by the inlet effect in Fig.3b. As the CO_2 heat transfer coefficient drops rapidly, it causes the heat flux to fall into the stabilization process. The rapid increase in the heat transfer coefficient of CO_2 is attributed to the bulk temperature of CO_2 approaching the critical point during the cooling process, where the physical properties of CO_2 change dramatically and the specific heat dominates the heat transfer process, causing the heat transfer coefficient to have the same trend as the specific heat. As mentioned before, the specific heat increases in the $T_b<T_{pc}$ and decreases in the region of $T_b>T_{pc}$. Although the CO_2 heat transfer coefficient and the total heat transfer coefficient increase, the temperature difference keeps dropping, so the heat flux also tends to decrease slightly. As the CO_2 temperature decreases, the CO_2 undergoes a phase change from a supercritical to a subcritical state, causing the heat flux to drop further until there is a slight rebound at the water inlet. That may be due to the high heat transfer coefficient of water at the water inlet. The heat transfer coefficient of water is found to be as much as five times higher than that of CO_2 at the CO_2 outlet by calculation. The heat transfer process in DPHE is similar to the above.

Figure 3cd shows the heat transfer process in STHE, including axial temperature, axial heat flux, and axial CO_2 heat transfer coefficient. The global heat transfer process in STHE is clearly distinguished from the heat transfer process in CPHE. First of all, the heat flux changes more drastically than that in CPHE, which is more attributed to the difference in the structure. The baffles in STHE changes the direction of water flow in the shell side. The presence of the baffles in STHE makes the heat flux change

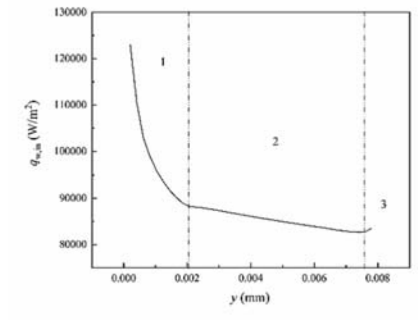

(a) Heat flux of the CPHE inner wall

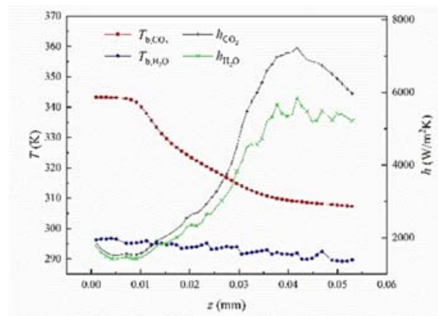

(b) Temperature distribution along the CPHE tube

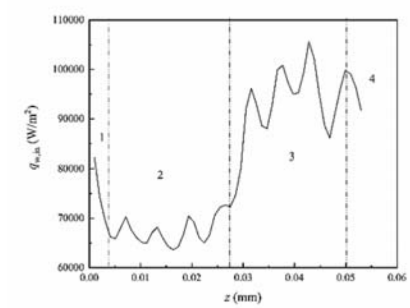

(c) Heat flux of the STHE inner wall

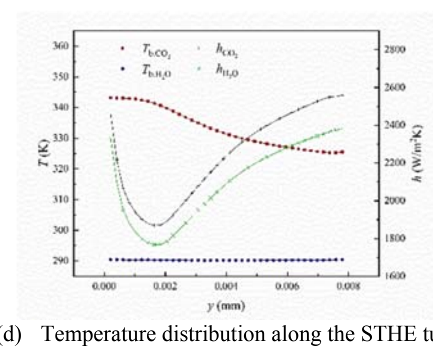

(d) Temperature distribution along the STHE tube

Fig. 3. Global heat transfer process in CPHE and STHE. ($G_{co_2,in}=100$ kg / m^{2}s, $G_{water}=1000$ kg / m^{2}s, $T_{water,in}=288.15$ K, $T_{co_2,in}=343.15$ K, P=8 MPa)

more drastically along the axial direction. Still, the whole process can be roughly divided into four parts: CO_2 inlet section, lower section, higher section, and water inlet section, as shown in Fig. 3c. Similarly, the high heat flux at the inlet is caused by the vast temperature difference between the refrigerant and cooling water, as shown in Fig. 3d. As the CO_2 heat transfer coefficient drops and rises, as shown in Fig. 3d, the temperature difference between the refrigerant and cooling water barely changes, causing the heat flux to decrease into the lower section. As the CO_2 temperature decreases, the CO_2 heat transfer coefficient increases dramatically again into the higher section attributed to the falling slowly temperature difference between the refrigerant and cooling water for the same reason the dramatically changing specific heat of CO_2. The temperature difference does not continue to decrease, and the CO_2 heat transfer coefficient and heat flux both reach their peak until the water inlet. It is obvious that the heat transfer process is entirely different for different structures of heat exchangers. Therefore, it is vital to analyze the global heat exchanger heat transfer process in order to design an efficient and compact heat exchanger. Baffles should be considered in the design of microchannel heat exchangers by comparing the heat transfer processes of CPHE and STHE. In addition, the global analysis of the heat exchanger shows that the heat transfer coefficient of CO_2 and water keeps changing all the time, which is noteworthy. The heat transfer characteristics of supercritical CO_2 in a heat exchanger are worth studying in order to design an efficient and compact heat exchanger.

3.2 s-CO_2 Heat Transfer Characteristics

3.2.1 Effects of Pressure

The operating pressure range of the heat exchanger in a trans-critical CO_2 refrigeration cycle is mostly 8-10 MPa. This pressure range was investigated in this study. The trend of heat transfer coefficient at different pressures is shown in Fig. 4. It is clear that when $T_{b,CO_2} < T_{pc}$, the rise in T_{b,CO_2} is accompanied by an increase in the heat transfer coefficient, which reaches a maximum when T_{b,CO_2} is a little bit higher than the pseudo-critical temperature, the heat transfer coefficient curve begins to decline as T_{b,CO_2} continues to rise. Higher peak heat transfer coefficients can be achieved at higher pressures.

This is consistent with the trend in specific heat, and it is easy to see that this is attributed to a dramatic change in specific heat. No significant difference in the peak of CO_2 heat transfer coefficients at different pressures for the three heat exchangers. A new reference temperature was defined to estimate the temperature at which the peak heat transfer coefficient of CO_2 occurs (Cai *et al.* 2020b), which was calculated by

$$T_{r,CO_2} = 0.8 \times T_b + 0.2 \times T_w$$

This equation is used to estimate the location of the peak CO_2 heat transfer coefficient occurrence before the post-processing, and the simulation results are consistent with the estimated value.

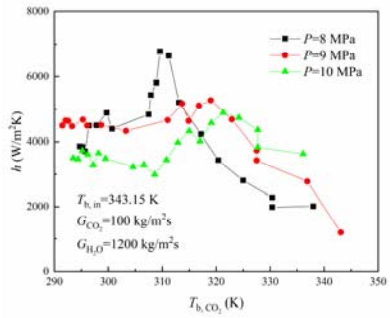

(a) DPHE

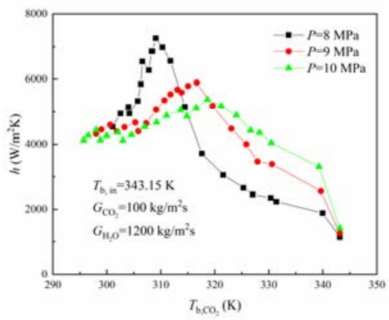

(b) CPHE

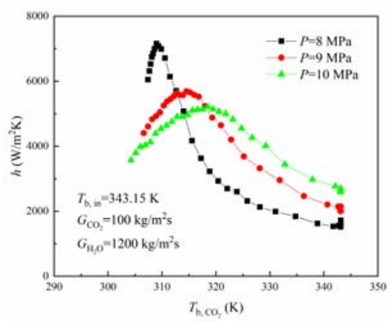

(c) STHE

Fig. 4. The h_{CO_2} at different pressure.

($G_{co_2,in} = 100\,\mathbf{kg/m^2s}$, $G_{water} = 1200\,\mathbf{kg/m^2s}$, $T_{water,in} = 288.15\,\mathbf{K}$, $T_{co_2,in} = 343.15\,\mathbf{K}$,)

3.2.2 Effects of CO_2 Mass Flux

Different CO_2 mass fluxes on the heat transfer coefficient cannot be underestimated. Figure 5 shows the trend of the CO_2 heat transfer coefficient at different CO_2 mass fluxes. It was found that increased refrigerant mass flux always results in larger heat transfer coefficients. The peak of the heat transfer coefficient also occurs at temperatures slightly above the critical temperature. Obviously, a higher heat transfer coefficient and lower CO_2 outlet temperature in DPHE can be obtained at the same CO_2 inlet temperature and operating pressure. The peak CO_2 heat transfer coefficients of all three heat exchangers occur at similar temperatures, indicating that this is entirely dominated by the CO_2 heat transfer characteristics and is not related to the heat exchanger structure.

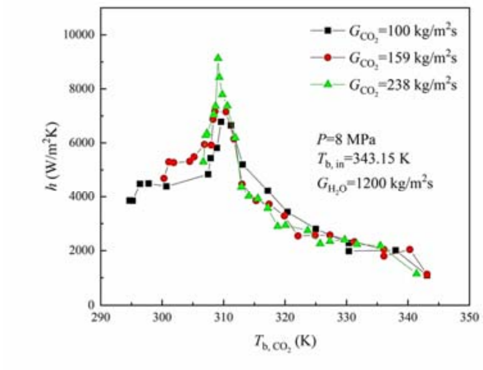

(a) DPHE

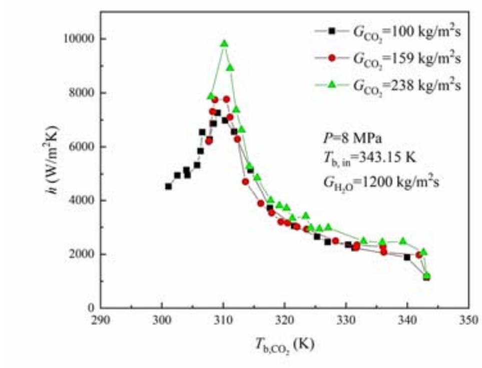

(b) CPHE

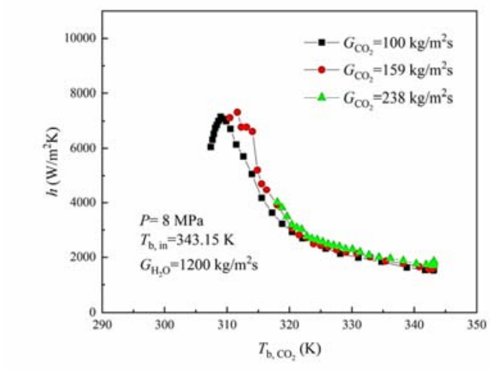

(c) STHE

Fig. 5. The h_{CO_2} at different G_{CO_2}.

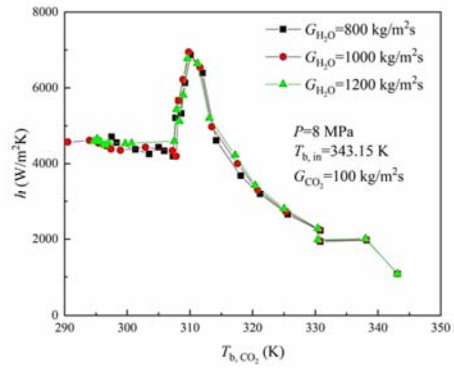

(a) DPHE

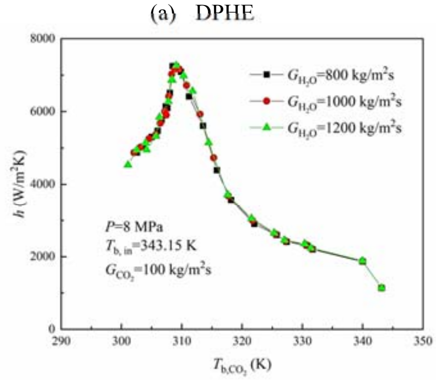

(b) CPHE

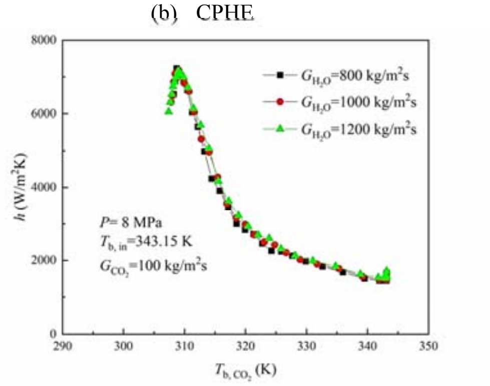

(c) STHE

Fig. 6. The h_{CO_2} at different G_{H_2O}.

3.2.3 Effects of Water Mass Flux

The trend of heat transfer coefficient at different water mass fluxes is shown in Fig. 6. It is expected that at high Reynolds numbers, the mass flux of water hardly affects the heat transfer process. Slightly in the $T_b<T_{pc}$ region, the reason why high water mass fluxes have high heat transfer coefficients are attributed to the vast temperature difference at the inlet. As the global heat transfer process proceeds, the temperature difference between the refrigerant and cooling water falling slowly, the CO_2 heat transfer coefficient almost does not change.

3.2.4 Effects of Gas Cooler Inlet Temperature

The trend of heat transfer coefficient at different heat exchanger inlet temperatures is shown in Fig. 7. The heat transfer coefficient first drops significantly, then increases to the first peak in the $T_b<T_{pc}$ region and reaches the second peak at a slightly higher than the pseudo-critical temperature, as can be shown in Fig. 7a and Fig. 7b. Both DPHE and CPHE show heat transfer coefficient fluctuations that occur in the subcritical region, while STHE does not show the situation described above due to its poor cooling effect and higher gas cooler outlet temperature than DPHE and CPHE, as can be seen in Fig. 7c.

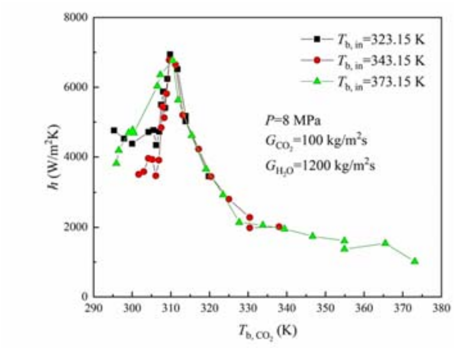

(a) DPHE

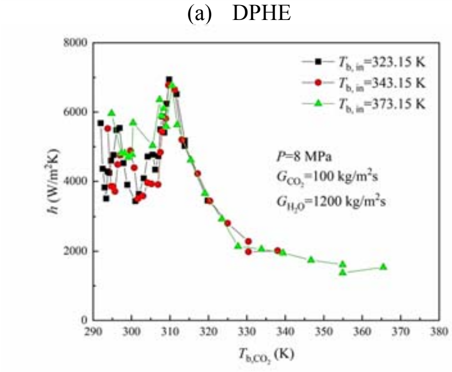

(b) CPHE

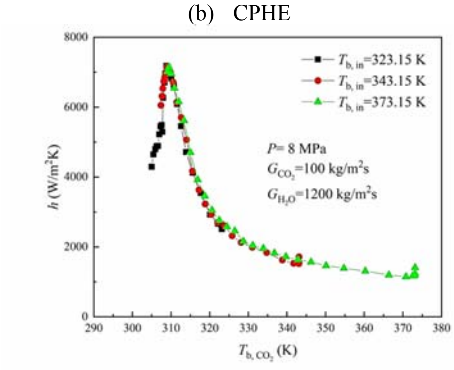

(c) STHE

Fig. 7. The h_{CO_2} at different $T_{b,in}$.

3.3 Effects of structure

The comparison of the supercritical CO_2 heat transfer characteristics of the three types of gas coolers in section 3.2 is equivalent to comparing the heat transfer characteristics of supercritical CO_2 in the horizontal spiral micro-tube, a horizontal serpentine micro-tube, and a horizontal straight micro-tube, where it is clear that the different flow patterns lead to different heat transfer effects. Similarly, the study of the complicated flow on the waterside is also essential for the design of micro-channel gas coolers due to the inhomogeneity of CO_2 properties derived from section 3.2. In this paper, the heat transfer effects of three heat exchangers were compared, and the results are shown in Table 3.

It can be found that the DPHE heat exchange effect is better than CPHE and STHE with the same heat transfer area on the CO_2 side. In fact, Guo *et al.* (2019) found that the cooling conditions spiral tube heat transfer effect is better than the straight tube, similarly Zheng *et al.* (2019) found that the serpentine tube heat transfer effect is better than the straight tube; the conclusion reached in this paper is that the heat transfer effect spiral tube is the strongest, followed by the serpentine tube, the worst is the straight tube. Figure 8 shows the temperature distribution at the outlet cross-section for each of the three different flow types at different operating conditions. The supercritical CO_2 near the inner wall is cooled first. It is found that DPHE always obtains the lowest outlet temperature for the same operating conditions. The structure of spiral double-pipe counter-current flow can effectively cool CO_2.

4. CONCLUSION

In this study, the heat transfer process between CO2 and water in three different structures of micro-channel heat exchangers was investigated in detail, and numerical simulations were performed to compare and analyze the three heat exchangers.

The heat transfer processes of the three heat exchangers were analyzed in detail.

Table 1 The $Q_{exchange}$ of three heat exchangers.

Q (W)	G_{co_2} (kg / m²s)			G_{water} (kg / m²s)			$T_{b,in}$ (K)			P (MPa)		
	100	159	238	800	1000	1200	323.15	343.15	373.15	8	9	10
STHE	13.2	13.5	13.5	11.8	12.4	13.2	12.4	15.2	18.3	13.2	14.3	14.4
CPHE	17.4	19.1	20.0	16.7	16.6	17.4	13.2	17.4	18.2	17.4	16.6	16.0
DPHE	18.2	29.5	36.4	19.7	21.0	18.2	14.4	19.8	24.6	18.2	18.0	15.8

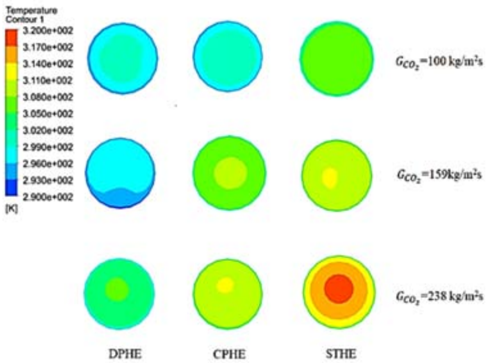

(a) Temperature variation at different G_{CO_2}

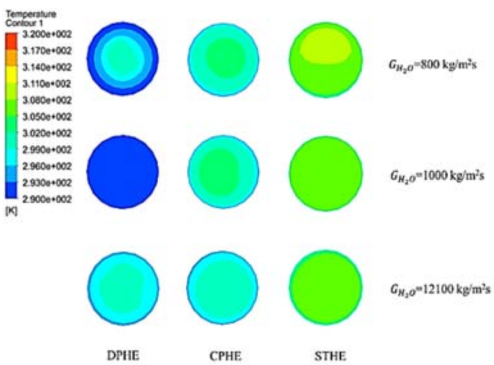

(b) Temperature variation at different G_{H_2O}

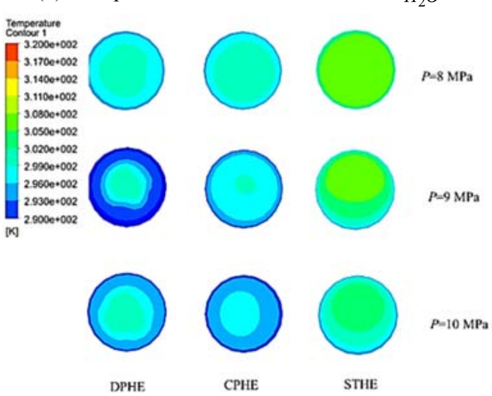

(c) Temperature variation at different P

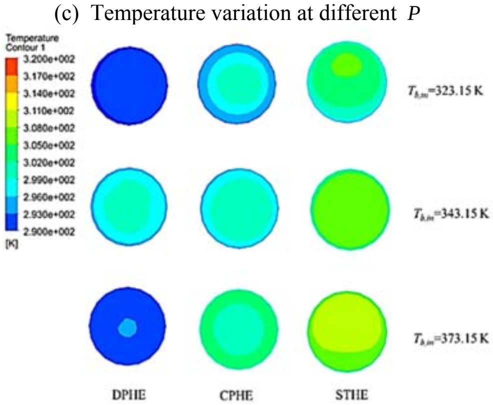

(d) Temperature variation at different $T_{b,in}$

Fig. 8. Temperature distribution at the outlet.

The effects of CO_2 pressure, the mass flux of CO_2, the mass flux of water, heat exchanger inlet temperature, and different flow patterns between CO_2 and water on the heat transfer effectiveness of the heat exchanger were considered. The following conclusions were drawn from this study.

1. The heat transfer process is entirely different for different structures of heat exchangers. Baffles should be considered in the design of microchannel heat exchangers. The heat transfer coefficient of CO_2 and water keeps changing all the time.

2. Increased refrigerant mass flux always results in more significant heat transfer coefficients. The peak of the heat transfer coefficient also occurs at temperatures slightly above the critical temperature, while the mass flux of water hardly affects the heat transfer process at high mass flux.

3. The heat transfer coefficient in CTHE first decreases significantly in the subcritical region thermal coefficient, then rises to the first peak in the region where the CO_2 bulk temperature is below the pseudo-critical temperature and reaches the second peak at the pseudo-critical temperature with different inlet temperatures, which is not present in DPHE and STHE.

4. DPHE has the best heat transfer effect, followed by CTHE, and the worst STHE and DPHE always obtains the lowest outlet temperature for the same operating conditions.

ACKNOWLEDGEMENTS

This paper is supported by this research has been supported by Science and technology innovation action plan of Shanghai Science and Technology Commission ((19DZ1207503).

REFERENCES

Bennett, K. and Y. Chen. (2020). One-way coupled three-dimensional fluid-structure interaction analysis of zigzag-channel supercritical CO2 printed circuit heat exchangers. *Nuclear Engineering and Design* 358, 110434.

Cai, H. fei, Y. yan Jiang, T. Wang, S. qiang Liang and Y. ming Zhu. (2020a). Experimental investigation on convective heat transfer and pressure drop of supercritical CO2 and water in microtube heat exchangers. *International Journal of Heat and Mass Transfer* 163, 120443.

Cai, H. fei, S. qiang Liang, C. hong Guo, T. Wang, Y. ming Zhu and Y. yan Jiang. (2020b). Numerical investigation on heat transfer of supercritical carbon dioxide in the microtube heat exchanger at low reynolds numbers. *International Journal of Heat and Mass Transfer* 151, 119448.

Chen, W., Z. Yang, L. Yang and M. K. Chyu. (2018). Numerical investigation of heat transfer and flow characteristics of supercritical CO_2 in Uduct. *Applied Thermal Engineering* 144, 532–539.

Ehsan, M. M., Z. Guan and A. Y. Klimenko. (2018). A comprehensive review on heat transfer and pressure drop characteristics and correlations with supercritical CO2 under heating and cooling applications. In *Renewable and Sustainable Energy Reviews* 92, 658–675.

Eskandari Manjili, F. and M. Cheraghi. (2019). Performance of a new two-stage transcritical CO2 refrigeration cycle with two ejectors. *Applied Thermal Engineering* 156, 402–409.

Fronk, B. M. and S. Garimella. (2011). Water-coupled carbon dioxide microchannel gas cooler for heat pump water heaters: Part II - Model development and validation. *International Journal of Refrigeration* 34(1), 17–28.

Guo, J., M. Xiang, H. Zhang, X. Huai, K. Cheng and X. Cui. (2019). Thermal-hydraulic characteristics of supercritical pressure CO2 in vertical tubes under cooling and heating conditions. *Energy* 170, 1067–1081.

Guoqing, S. (2015). Study on fluid flow and heat transfer in a mini channel tube-in-tube heat exchanger. *In Chinese*.

Han, Y., Y. Liu, M. Li and J. Huang. (2012). A review of development of micro-channel heat exchanger applied in air-conditioning system. *Energy Procedia* 14, 148–153.

Jiang, P. X., Y. Zhang and R. F. Shi. (2008). Experimental and numerical investigation of convection heat transfer of CO2 at supercritical pressures in a vertical mini-tube. *International Journal of Heat and Mass Transfer* 51(11–12), 3052–3056.

Jiang, P. X., Y. Zhang, Y. J. Xu and R. F. Shi. (2008). Experimental and numerical investigation of convection heat transfer of CO2 at supercritical pressures in a vertical tube at low Reynolds numbers. *International Journal of Thermal Sciences* 47(8), 998–1011.

Jiang, P. X., Y. Zhang, C. R. Zhao and R. F. Shi. (2008). Convection heat transfer of CO2 at supercritical pressures in a vertical mini tube at relatively low reynolds numbers. *Experimental Thermal and Fluid Science* 32(8), 1628–1637.

Katz, A., S. R. Aakre, M. H. Anderson and D. Ranjan. (2021). Experimental investigation of pressure drop and heat transfer in high temperature supercritical CO2 and helium in a printed-circuit heat exchanger. *International Journal of Heat and Mass Transfer* 171, 121089.

Kim, M. H. and C. W. Bullard. (2001). Development of a microchannel evaporator model for a CO2 air-conditioning system. *Energy* 26(10), 931–948.

Kim, S. G., Y. Lee, Y. Ahn and J. I. Lee. (2016). CFD aided approach to design printed circuit heat exchangers for supercritical CO2 Brayton cycle application. *Annals of Nuclear Energy* 92, 175–185.

Lei, X., J. Zhang, L. Gou, Q. Zhang and H. Li. (2019). Experimental study on convection heat transfer of supercritical CO2 in small upward channels. *Energy* 176, 119–130.

Li, J., J. Jia, L. Huang and S. Wang. (2017). Experimental and numerical study of an integrated fin and micro-channel gas cooler for a CO2 automotive air-conditioning. *Applied Thermal Engineering* 116, 636–647.

Liang, Y., Z. Sun, M. Dong, J. Lu and Z. Yu. (2020). Investigation of a refrigeration system based on combined supercritical CO2 power and transcritical CO2 refrigeration cycles by waste heat recovery of engine. *International Journal of Refrigeration* 118, 470–482.

Ma, T., W. X. Chu, X. Y. Xu, Y. T. Chen and Q. W. Wang. (2016). An experimental study on heat transfer between supercritical carbon dioxide and water near the pseudo-critical temperature in a double pipe heat exchanger. *International Journal of Heat and Mass Transfer* 93, 379–387.

Nekså, P., H. Rekstad, G. R. Zakeri and P. A. Schiefloe. (1998). CO2-heat pump water heater: Characteristics, system design and experimental results. *International Journal of Refrigeration* 21(3), 172–179.

Pan, M., X. Bian, Y. Zhu, Y. Liang, F. Lu and G. Xiao. (2020). Thermodynamic analysis of a combined supercritical CO2 and ejector expansion refrigeration cycle for engine waste heat recovery. *Energy Conversion and Management* 224, 113373.

Rigola, J., G. Raush, C. D. Pérez-Segarra and A. Oliva. (2005). Numerical simulation and experimental validation of vapour compression refrigeration systems. Special emphasis on CO2 trans-critical cycles. *International Journal of Refrigeration* 28(8), 1225–1237.

Saeed, M., A. S. Berrouk, M. Salman Siddiqui and A. Ali Awais. (2020). Numerical investigation of thermal and hydraulic characteristics of sCO2-water printed circuit heat exchangers with zigzag channels. *Energy Conversion and Management* 224(August), 113375.

Sanaye, S., N. Khakpaay, A. Chitsaz, M. Hassan Yahyanejad and M. Zolfaghari. (2020). A comprehensive approach for designing, modeling and optimizing of waste heat recovery cycle and power generation system in a cement plant: A thermo-economic and environmental assessment. *Energy Conversion and Management*, 205(September 2019), 112353.

Soloveva, O., S. Solovev and R. Yafizov. (2021). Hydrodynamics and Convective Heat Transfer in Open Cell Foam with Micropores. *Transportation Research Procedia* 54, 64–68.

Wang, D., B. Yu, W. Li, J. Shi and J. Chen. (2018). Heating performance evaluation of a CO2 heat pump system for an electrical vehicle at cold ambient temperatures. *Applied Thermal Engineering* 142(July), 656–664.

Wang, H. and S. M. Kissick. (2020). Modeling and simulation of a supercritical CO2-liquid sodium compact heat exchanger for sodium-cooled fast reactors. *Applied Thermal Engineering* 180, 115859.

Wang, Q., Z. Song, Y. Zheng, Y. Yin, L. Liu, H. Wang and J. Yao. (2019). Coupled convection heat transfer of water in a double pipe heat exchanger at supercritical pressures: An experimental research. *Applied Thermal Engineering* 159, 113962.

Xu, R. N., F. Luo and P. X. Jiang. (2015). Experimental research on the turbulent convection heat transfer of supercritical pressure CO2 in a serpentine vertical mini tube. *International Journal of Heat and Mass Transfer* 91, 552–561.

Yang, D., J. Xie, J. Lv and J. Wang. (2017). An Experimental and Numerical Study of Helix Tube Gas Cooler for Super-Critical Carbon Dioxide. *Journal of Chemical Engineering of Japan* 50(12), 900–908.

Yang, J., B. Yu and J. Chen. (2019). Improved genetic algorithm-based prediction of a CO2 micro-channel gas-cooler against experimental data in automobile air conditioning system. *International Journal of Refrigeration* 106, 517–525.

Yang, Z., W. Chen and M. K. Chyu. (2018). Numerical study on the heat transfer enhancement of supercritical CO2 in vertical ribbed tubes. *Applied Thermal Engineering* 145, 705–715.

Zhang, S., X. Xu, C. Liu, X. Liu, Z. Ru and C. Dang. (2020). Experimental and numerical comparison of the heat transfer behaviors and buoyancy effects of supercritical CO2 in various heating tubes. *International Journal of Heat and Mass Transfer* 149.

Zhang, Y., M. Peng, G. Xia and T. Cong. (2019a). Numerical investigation on local heat transfer characteristics of S-CO2 in horizontal semicircular microtube. *Applied Thermal Engineering* 154, 380–392.

Zheng, Y., P. X. Jiang, F. Luo and R. N. Xu. (2019b). Instability during transition to turbulence of supercritical pressure CO2 in a vertical heated serpentine tube. *International Journal of Thermal Sciences* 145(September 2018), 105976.

Zhu, Y., Y. Huang, S. Lin, C. Li and P. Jiang. (2019). Study of convection heat transfer of CO2 at supercritical pressures during cooling in fluted tube-in-tube heat exchangers. *International Journal of Refrigeration* 104, 161–170.